Korean J. Chem. Eng., 35(11), 2164-2171 (2018)
DOI: 10.1007/s11814-018-0141-6

pISSN: 0256-1115
eISSN: 1975-7220

Evaluation of the cavitation effect on liquid fuel atomization by numerical simulation

Sang In Choi*, Jia Ping Feng*, Ho Suk Seo, Young Min Jo*,†, and Hyun Chang Lee*****

*Department of Applied Environmental Science, Kyung Hee University, Yongin 17104, Korea
**EG Power Tech Co., Ltd., Suwon 16229, Korea
***Dept. of Mechanical Design, Kangwon National University, Samcheok 25913, Korea
(*Received 16 February 2018 • accepted 16 August 2018*)

Abstract−Heavy duty diesel vehicles deteriorate urban air quality by discharging a large volume of air pollutants such as soot and nitrogen oxides. In this study, a newly introduced auxiliary device a fuel activation device (FAD) to improve the combustion efficiency of internal engines by utilizing the cavitation effect was closely investigated by the fluid flow mechanism via a numerical analysis method. As a result, the FAD contributed to fuel atomization from the injection nozzle at lower inlet pressure by reducing the pressure energy. The improved cavitation effect facilitated fuel atomization, and ultimately reduced pollutant emission due to the decrease in fuel consumption. The axial velocity along the flow channel was increased 8.7 times with the aid of FAD, which improved the primary break-up of bubbles. The FAD cavitation effect produced 1.09-times larger turbulent bubbles under the same pressure and fuel injection amount than without FAD.

Keywords: Diesel Engine, Fuel Activation Device, Cavitation, Cavitation Number, CFD

INTRODUCTION

Particulate matter (PM), nitrogen oxides (NOx) and carbon monoxide (CO) from mobile emissions are considered serious air pollutants in urban areas. They account for 31% of the total NOx emissions in Korea (2013) and 39% in Europe (2014) [1]. Diesel engines, which are ignited by compression of fuel, discharge approximately 30 to 100 times more emission than gasoline engines [2]. The International Agency for Research on Cancer (IARC) classified the pollutants from diesel engines as primary carcinogenic materials [3]. In particular, a large number of old engines on heavy trucks, buses and trains manufactured before the recent common rail direct injection (CRDI) system are still on the road [4]. Heavy vehicles are compelled to install a diesel particulate filter (DPF) by law. Although the DPF materials such as SiC or a ceramic monolith are very anticorrosive and highly efficient at filtration, they are costly and apt to break when regeneration occurs due to overheating. DPF materials also have the problem of periodic replacement to prevent pressure build by accumulating dust [5].

To compensate for such disadvantages, an auxiliary fuel activated device (FAD; EG Powertech Co. Ltd., Korea) was developed and inserted into the connecting tubes of the nozzles of a diesel fuel tank [4,6]. The FAD reduces the injected droplet size by the physical mechanism of atomization and contributes to combustion efficiency, ultimately resulting in decreased emission of the particulate matter and gaseous pollutants. Compared to DPF, the FAD shows a very long lifetime and different approach, applying a prior step to the engine combustion.

The number of fine droplets in the same volume of liquid fuel was determined by an atomization effect. The smaller the droplets, the total number of droplets increases. The number of fine droplets relates with the combustion efficiency by providing a unit surface area that contacts air flow [7]. The split in fuel droplets and turbulence could be enhanced by the cavitation effect in driving tools or structures. This effect improves the primary breakup of liquid fuel, which facilitates atomization [8]. The practical effectiveness of FAD was evaluated in trains in Mongolia [6], and the cavitation phenomenon was experimentally investigated in terms of fuel injection distance with various nozzles [4].

This study examines the fluid flow behavior in FAD with computational fluid dynamics (CFD) using a commercial code (Fluent v.18.0, Ansys Work bench, USA). The main principle of atomization by FAD was closely traced, and the cavitation effect was examined depending on the inlet pressure.

CALCULATION MODELS FOR NUMERICAL ANALYSIS

We used a commercial CFD code (Fluent v.18.0, ANSYS, USA) to perform the numerical simulation while observing the cavitation effect and turbulent phenomena inside the nozzle. Since the flow behavior of the two-phase fluids including liquid and gas must be determined to evaluate the cavitation effect, the mixture model was thought to be appropriate. The mixture model is effective for the multi-phase flow because it assumes homogeneous mixing of the two phases [9]. The LES model is a turbulent model that shows high accuracy in an unsteady state. The Schnerr-Sauer model, which is compatible with the large eddy simulation (LES) model, was used to investigate the cavitation effect.

1. Large Eddy Simulation (LES) Modeling

The LES model is often used to predict and understand the unsteady flow of diesel fuel injection with high accuracy [10-13], and

†To whom correspondence should be addressed.
E-mail: ymjo@khu.ac.kr

is very useful in the analysis of cavitation flow and the formation at the throttle and injectors. The LES model is cost-effective and simple enough to calculate complex configurations by obtaining more information under turbulent conditions [9,14].

The LES model based on the continuous Eq. (1) and Navier-Stokes Eq. (2) employed the Smagorinsky-Lilly model [9,10]. The subgrid-scale stress (SGS; τ_{ij}) in Eq. (2) was defined according to Eqs. (3) and (4):

$$\frac{\partial \rho}{\partial t} + \frac{\partial}{\partial x_i}(\rho \bar{u}_i) = 0 \tag{1}$$

$$\frac{\partial}{\partial t}(\rho \bar{u}_i) + \frac{\partial}{\partial x_j}(\rho \bar{u}_i \bar{u}_j) = -\frac{\partial \bar{P}}{\partial x_j} + \frac{\partial}{\partial x_j}\left(\mu \frac{\partial \bar{u}_i}{\partial x_j}\right) - \frac{\partial \tau_{ij}}{\partial x_j} \tag{2}$$

$$\tau_{ij} - \frac{1}{3}\tau_{kk}\delta_{ij} = -2\mu_t \bar{S}_{ij} \tag{3}$$

$$\bar{S}_{ij} = \frac{1}{2}\left(\frac{\partial \bar{u}_i}{\partial x_j} + \frac{\partial \bar{u}_j}{\partial x_i}\right) \tag{4}$$

The eddy viscosity (μ_t) in the Smagorinsky-Lilly model was defined as:

$$\mu_t = \rho L_s^2 \sqrt{2\bar{S}_{ij}\bar{S}_{ij}} \tag{5}$$

$$L_s = \min(\kappa d, C_s V^{1/3}) \tag{6}$$

where, L_s indicates the mixing ratio of the sub-grid scales, κ is the von Karman constant, C_s is the Smagorinsky constant, V is the volume of the computational cells, and d represents the distance between neighboring walls.

2. Modeling of Cavitation Effect

Cavitation flow was simulated using Schnerr and Sauer model [15], which corresponds to the LES turbulence model and is well suited to delicate orifice design [9,15,16]. To achieve an accurate expression for mass transfer of liquid and vapor, this model uses the following two-phase continuity relation of the Vapor Transport Eq. (7):

$$\frac{\partial}{\partial t}(\alpha \rho_v) + \nabla \cdot (\alpha \rho_v \vec{V}) = R_e - R_c \tag{7}$$

where ρ_v is vapor density, R_e and R_c represent the formation rate and decay rate of bubbles respectively. α is the volume fraction of vapor and can be obtained as follows:

$$\alpha = \frac{n \cdot 4\pi R_B^3/3}{1 + n \cdot 4\pi R_B^3/3} \tag{8}$$

The Schnerr and Sauer model based on the Rayleigh Plesset equation presents bubble formation and decay caused by the cavitation effect according to Eqs. (9) and (10) [15]:

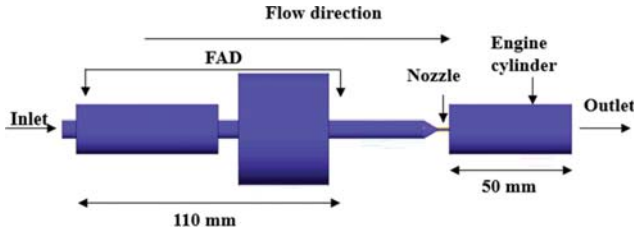

Fig. 1. 3D schematic diagram of the test FAD.

$$R_e = \frac{\rho_v \rho_l}{\rho} \alpha (1-\alpha) \frac{3}{R_B} \sqrt{\frac{2(p_v - p)}{3 \rho_l}} \quad (p_v \geq p) \tag{9}$$

$$R_c = \frac{\rho_v \rho_l}{\rho} \alpha (1-\alpha) \frac{3}{R_B} \sqrt{\frac{2(p - p_v)}{3 \rho_l}} \quad (p_v \leq p) \tag{10}$$

where p_v and p mean saturated vapor pressure and static pressure, respectively, and R_B is the bubble diameter.

TEST DEVICE AND METHODS

1. Structure and Principles of FAD

Fig. 1 depicts a three-dimensional diagram of the test flow including FAD (PATENT-2015-0021792) for the present numerical simulation. The liquid fuel flows across two gears consisting of spiral slits and passes through a following small ring with a diameter that is reduced by half. The overall passage was designed with 177 mm long. The fuel fluid exiting the small ring enters a nozzle at which the fuel is injected into the engine cylinder. The FAD reduces the size of the large droplets (4, 5, 7.5, 10 μm) by 21.0, 33.8, 76.1 and 93.4% respectively [6]. This size reduction improves the combustion efficiency by increasing the surface area per unit volume of the injected fuel droplets, and thereby reduces fuel consumption. This mechanism ultimately resulted in a decrease in PM exhaust [17,18].

2. Operation Parameters and Test Variables

This numerical study attempted to understand the principle of the FAD by observing the flow behavior in the internal structure of the device. Properties of the test liquid fuel used in the simulation are summarized in Table 1. To compare the microscopic characteristics of the fuel injection, a single nozzle was inserted parallel to the flow path after the FAD [19,20]. Since a nozzle design along a straight line minimizes the cavitation effect due to the nozzle, the effect induced by FAD alone can be clearly evaluated. To differentiate from the conventional structure, the nozzle opening and length were scaled to 1 mm and 4 mm, respectively. The practical ratio of length versus opening diameter (=4 mm) and the combustion engine cylinder occupied a constant volume of (ϕ20 mm×50 mm). The cylinder behind the nozzle aided in convergence because of the stable calculation [22]. The inlet and outlet were established with a pres-

Table 1. Diesel fuel specification

Liquid phase		Vapor phase		Saturation pressure (pa)
Density (kg/m^3)	Dynamic viscosity (kg/m·s)	Density (kg/m^3)	Dynamic viscosity (kg/m·s)	
830	3×10^{-3}	9.4	7×10^{-6}	1250

Table 2. Specification of the operating boundary condition for numerical calculation

Parameter	Value
Injection pressure	~15 MPa
Back pressure	0.1, 3 MPa
Nozzle length	4 mm
Nozzle diameter	1 mm
Cylinder length	50 mm
Cylinder diameter	20 mm

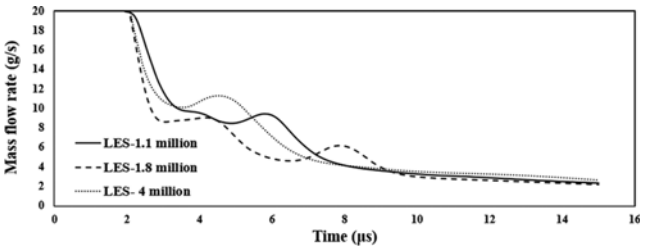

Fig. 2. Effect of grid number on the mass flow rate.

sure boundary condition and gravity was ignored. Other detailed conditions are summarized in Table 2.

Since the grid density in the numerical analysis influences the accuracy of the calculation, the mass flow rate discharged from the outlet was first evaluated in terms of the number of grids, as shown in Fig. 2. According to the preliminary result, the mass flow rate was substituted by 2.3, 2.1, and 2.6 g/s for 1.1 million, 1.8 million, and 4 million grids, respectively.

RESULTS AND DISCUSSION

1. Principle of FAD

A basic investigation of the pressure distribution, flow rate, viscosity variation and cavitation formation was first performed in a reference design without FAD for a consistent pressure condition (inlet pressure: 10 MPa, back pressure: 3 MPa). Then the effect of the cavitation by FAD installation was observed based on the numerical simulation.

1-1. Effect of FAD on Flow Pressure

Pressure variation across the flow path line was calculated with and without FAD, as described in Fig. 3. In the case without FAD, the internal pressure of the flow path consistently increased and finally reached 67 MPa, which was six-times greater than the inlet pressure. However, the pressure with FAD decreased as it passed through the two pairs of gears (8-42 mm), and further decreased as the fuel flowed through a small ring placed at 42 mm to 52 mm where the flow path cross area was reduced by half. The third pressure decrease was found at between 60 to 87 mm across the large ring. The internal pressure inside the large ring even with the tiny six slits was less than the vapor pressure of diesel fuel. Accordingly, the flow velocity was also very low, and cavitation did not occur. The pressure of the diesel flow after FAD again increased to the nozzle entrance, reaching the maximum 35 MPa, which was 3.5-times higher than the inlet pressure. The final pressure of the diesel flow entering the nozzle was half that of the case without FAD.

Since the turbulent flow field at the inner surface of the flow channel includes various patterns, the insertion of FAD induces complex changes in the fluid flow toward the nozzle at the solid boundary layer. Eq. (2) of the LES model in this study proved that the increase in shear stress decreased the total energy. The turbulent shear stress could be estimated by the eddy viscosity, which was obtained from Eq. (5). The overall frictional stress over the turbulent flow is expressed as the value with the addition of friction effects at the wall surface. However, this could be ignored because the liquid viscosity is much less than the eddy viscosity. As a result, the frictional stress in the turbulent flow could be determined by the eddy viscosity as shown in Eq. (3).

Fig. 4 shows the variation of the eddy viscosity due to the FAD. The intensity of the eddy viscosity was approximately 0.02 Pa·s at every boundary surface of which the fluid flow changed significantly. This change in fluid flow enhanced the shear stress and ultimately decreased the potential energy of the liquid fuel; therefore, the pressure change in the FAD was reduced as shown in Fig. 3.

1-2. Effect of FAD on Flow Velocity

The pressure reduction due to the eddy viscosity in FAD may lead to a flow velocity change by reduction of the potential energy of the liquid fuel. To analyze such behavior, the flow velocity variation along the channel axis was evaluated and summarized in Fig. 5.

Flow velocity is a parameter that plays an important role in cavitation formation at the nozzle besides pressure. The fluid moved to the nozzle at a constant velocity, 10 m/s in the reference case without FAD, and the velocity increased as it flowed through the inclined passage of 60°. In the case with FAD, the fuel's initial velocity of 18 m/s decreased while passing through the gear. However, pressure and flow velocity were not found in the vicinity of the gear in the

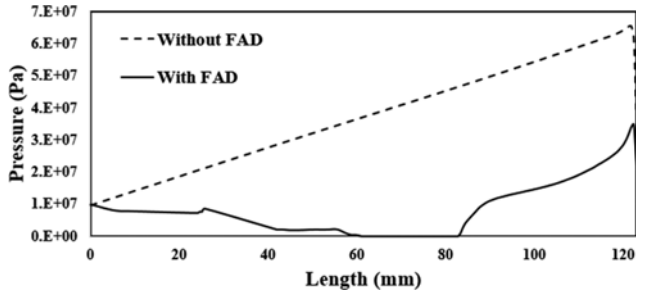

Fig. 3. Pressure variation across the flow path with and without FAD.

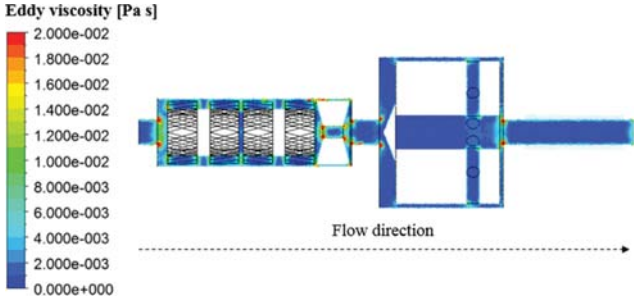

Fig. 4. Eddy viscosity variation in the FAD.

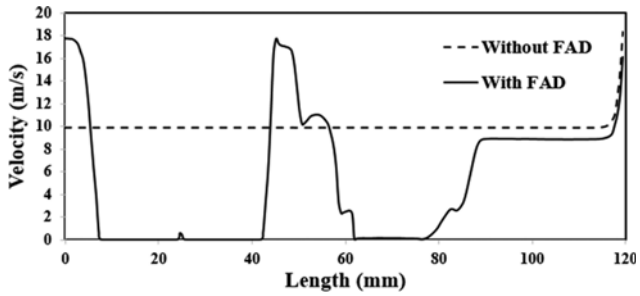

Fig. 5. Velocity profiles with and without FAD.

regime of 8 to 42 mm in Fig. 5 because the fluid flowed along the slits.

The internal pressure and velocity are shown in Fig. 6. The velocity was initiated at 8 m/s and decreased to 4 m/s depending on the load while passing through the gears. The pressure increased up to three-times more than the inlet pressure. It was also difficult to measure the velocity distribution in the axial direction when the fluid flowed along the side of the large ring. These parts are displayed in Fig. 7. In conclusion, diesel fluid with FAD entered the nozzle at a slightly low velocity, but the pressure was maintained at half of the reference design.

2. Flow Pattern Inside the Nozzle

Vigorous fluid flow resulted in the rapid decrease of pressure to less than the vapor pressure, as flow entered the nozzle after passing the FAD, so cavitation was therefore generated. The primary breakup in the fuel injection mechanism can be improved by turbulent effects, which are enhanced by cavitation [23]. This cavitation can be quantitatively evaluated as the fraction of the liquid fuel vapor [24].

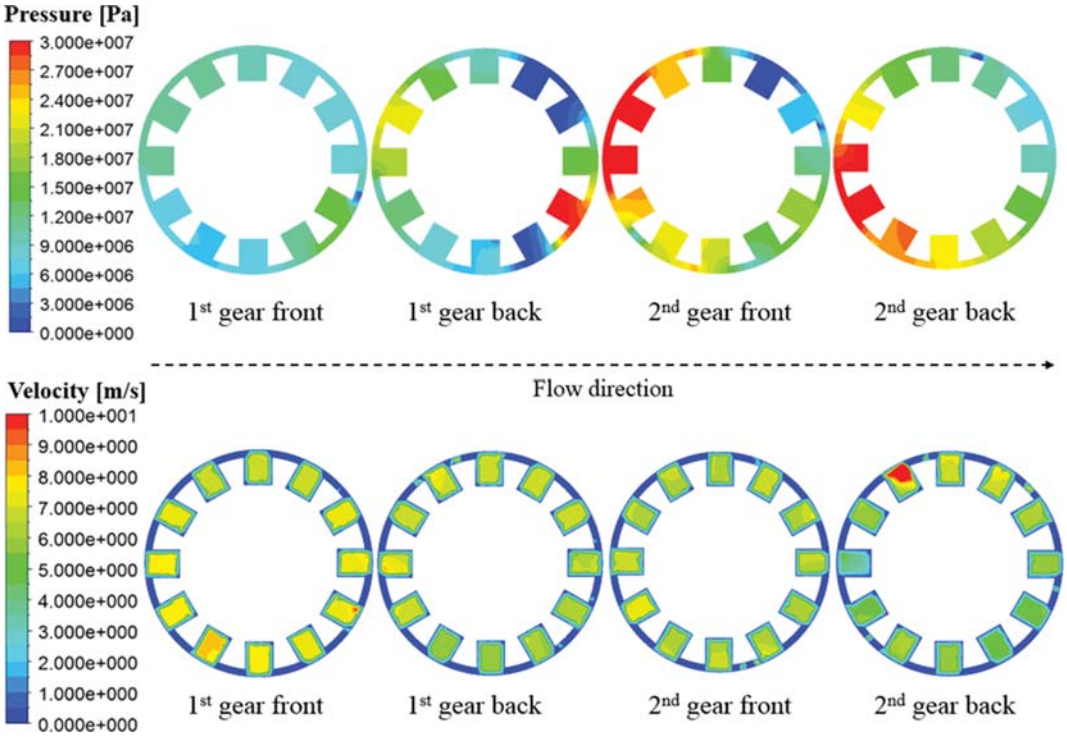

Fig. 6. Radial flow characteristics in the FAD (Length range: 8-42 mm).

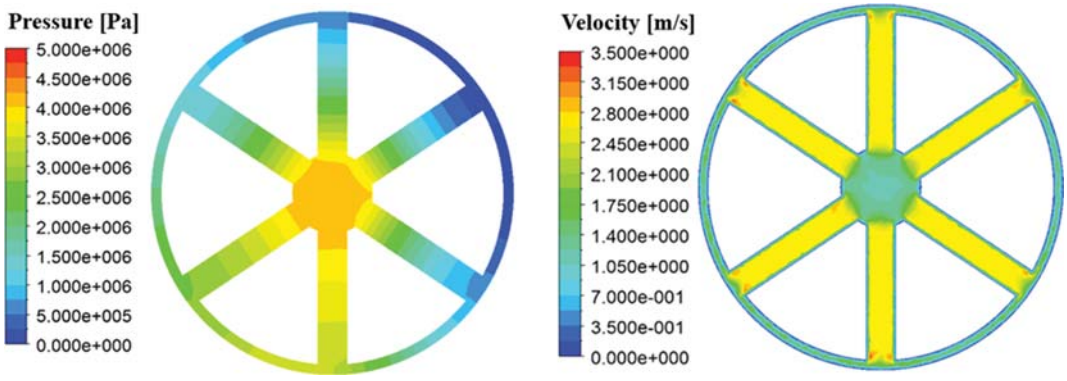

Fig. 7. Radial flow characteristics in the FAD (Length range: 60-87 mm).

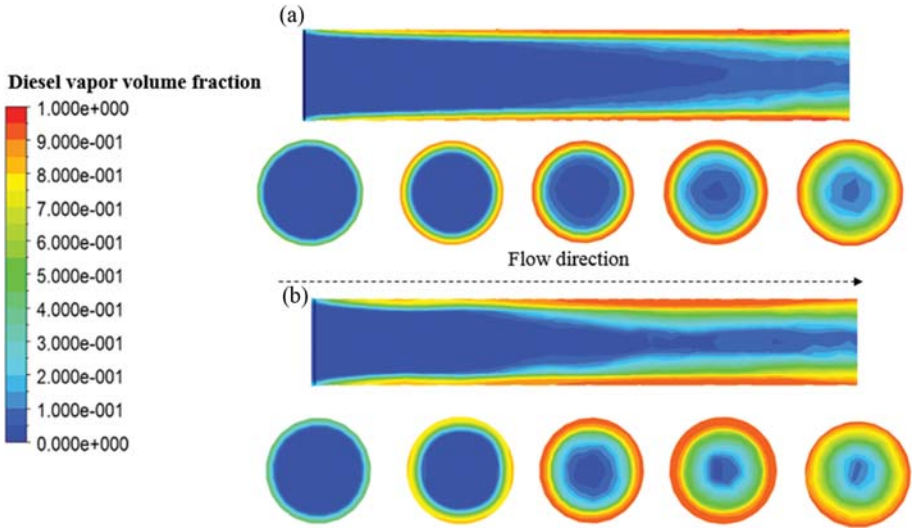

Fig. 8. Cavitation effect in the nozzle, (a) without FAD and (b) with FAD.

The vapor volume fraction is calculated by Eq. (8) and increases proportionally to the number of bubbles with the assumption that the bubble size is constant. Numerous bubbles resulted when the increased volume was converted to the liquid phase as the internal pressure of the nozzle finally exceeded the vapor pressure. At the same time, energy was discharged, initiating the primary break-up [25].

Fig. 8 describes the cavitation effect within the nozzle. The nozzle length was 4 mm, and the effect across the cross-sections of the nozzle was also investigated at the axial distance: 0, 1, 2, 3 and 4 mm. The increase in vapor volume fraction was approximately from 2 mm from the nozzle entrance by FAD. Cavitation was created from the boundary surface of the wall and propagated to the center of the nozzle when the flow entered the engine cylinder. Bubbles present in the wall boundary were apt to break only the liquid surface, but the mixed phase of liquid and vapor showed significant break-up, which may contribute to more atomization of the liquid fuel.

In addition, the enhanced cavitation effect reduced the friction against the wall surface, resulting in an increase in the flow velocity [26]. Fig. 9 is a graph showing the flow velocity profiles within the nozzle. The entering liquid fuel passes the nozzle at 345 m/s and 316 m/s without and with FAD, respectively. Despite similar initial velocities, the installation of the FAD increased the injection velocity up to 811 m/s, which was 1.2-times greater than the velocity without FAD, 673 m/s. This increased velocity could compensate for the reduction of the nozzle's hydraulic diameter, which forms more turbulence at the same flow rate, enhancing the atomization efficiency.

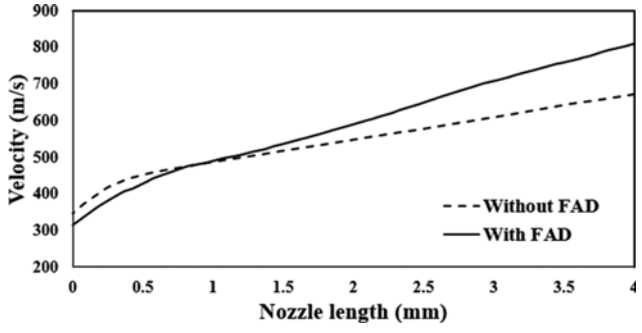

Fig. 9. Velocity variation at the nozzle inside with and without FAD installation.

The difference in the cavitation effect across the nozzle could be explained by Bernoulli's Eq. (11), where subscript a indicates the point before entering the nozzle and b is an arbitrary point inside the nozzle.

$$\frac{P_a}{\rho}+\frac{u_a^2}{2}+gZ_a=\frac{P_b}{\rho}+\frac{u_b^2}{2}+gZ_b \tag{11}$$

The potential energy terms could be negligible due to the same fluid pathway. With the assumption that the mass flow rate entering the nozzle is constant, the diameters at a and b are 6 mm and 1 mm, respectively, which confirms the velocity difference as 36-times. The substitution of the diesel density resulted in Eq. (12) as follows:

$$P_a-P_b=5.4\times10^5\cdot u_a^2[\mathrm{Pa}] \tag{12}$$

The pressure gradient increasing with the square of the velocity was less for the low pressure on the inside of the nozzle. A significant difference was found in the entering pressure toward the nozzle with and without FAD despite the similar velocity. As a result, the pressure inside the nozzle became low, and the cavitation effect increased more than the reference design without FAD. This result proved that a lower pressure liquid might form cavitation effects more easily at the same velocity.

The cavitation effect was numeralized based on many preliminary studies using Eq. (13) for quantitative assessment:

$$K_1=\frac{P_{in}-P_b}{P_b-P_v},\ K_2=\frac{P_{in}-P_v}{P_{in}-P_b},\ K_3=\frac{P_c-P_v}{\rho V_c^2/2} \tag{13}$$

Here, P_{in} is the inlet pressure, P_b is the back pressure, P_v is the vapor pressure of the test fluid, and P_c and V_c are the pressure and velocity of the point which decreased by axial flow respectively. In

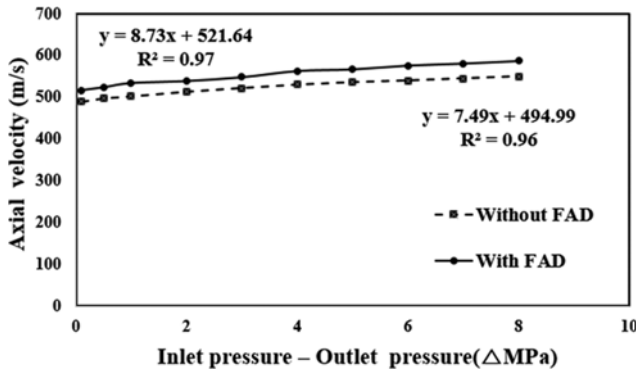

Fig. 10. Mean axial velocity inside the nozzle depending on pressure difference.

practice, many workers used numerical definitions of K_1, K_2 and K_3 to describe the cavitation effects in various fluid mechanics [27-31]. Considering that FAD could form the cavitation effect by the pressure difference at a similar velocity, we employed K_2 for the analysis of the cavitation number.

Fig. 10 shows the average axial velocities inside the nozzle in the presence of a pressure difference between the inlet and outlet. The axial velocity was higher with FAD than without for all inlet pressures. Thus, the cavitation effect can be improved with the aid of the FAD for all regimes of pressure. The axial velocity increases in the presence of a pressure difference were 7.5 and 8.7 without and with FAD, respectively. Thus the driving force from this pressure difference is greater with FAD than without.

The fuel injection amount is a significant factor to estimate the pressure loss and atomization efficiency that occur in a practical diesel engine chamber [23,30]. In particular, the pressure gradient in the FAD may lead to reduction of the injection amount; thus, the mass flow rate injected from the nozzle was evaluated relative to the inlet pressure, as shown in Table 3. As a result, the high pressure resulted in an increase in mass flow rate regardless of FAD installation. The mass difference with and without FAD was only ±1.4%. Thus, with the same amount of fuel, a faster driving velocity could be achieved with the FAD.

Table 3. Mass flow rate in the nozzle depending on inlet pressure

Inlet pressure - back pressure, ΔP (MPa)	Without FAD (g/s)	With FAD (g/s)
0.1	197	200
0.5	204	203
1	205	205
3	215	214
5	216	219
7	225	223

3. Cavitation Formation Inside the Nozzle with Inlet Pressure

The formation and development of cavitation in the nozzle with FAD were investigated in terms of inlet pressure [21,32]. As shown in Fig. 11, under the same condition of the inlet pressure, longer loci of the vapor flow at the inside surface of the nozzle occurred with the FAD. A long elliptical curvature shape often found in a single nozzle was developed when there was no FAD [13,33]. However a shape with injection angles which was observed in a valve cover orifice nozzle was formed [34-36]. In other words, the cavitation model illustrates that the instantaneous fluctuation of diesel fuel passing through the FAD was significant upon entering the nozzle. Therefore, the difference between the velocities on the x and y-axes led to fluid cavitation, even though the axial velocity (z-axis)

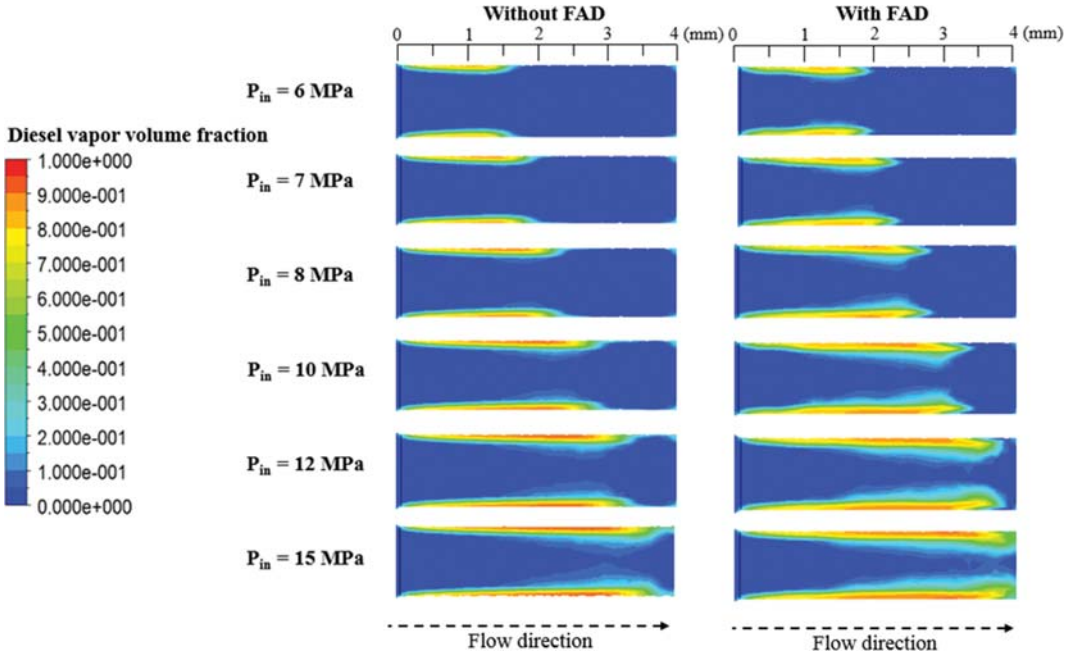

Fig. 11. Development steps of the cavitation in terms of the inlet pressure.

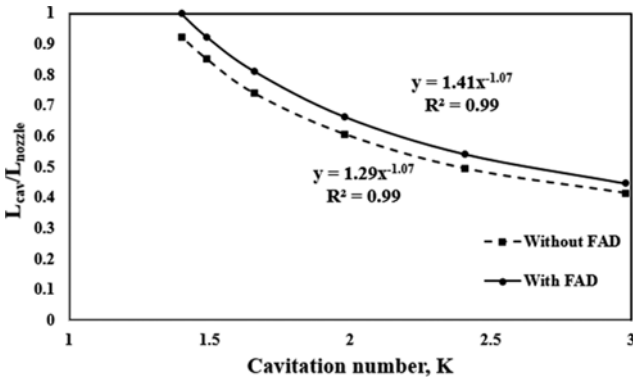

Fig. 12. Relation between the ratio of the cavitation length to the nozzle length with cavitation number.

remained similar to the case without FAD.

Most works on the cavitation effects in nozzles or injectors of diesel engines have focused on the nozzle or injector only [37,38]. However, this work attempted to trace the formation and development of cavitation throughout the flow channel based on quantitative evaluation. In accordance, the relative cavitation length to the nozzle was compared by cavitation number (K_2) as defined in Eq. (13). Fig. 12 approximates the relationship of the cavitation effect by FAD. Eqs. (14) without FAD and (15) with FAD indicate that the cavitation initiates development at a slightly lower pressure and forms a long tail. However, since the exponent values of both relations are very similar, the effect of cavitation by FAD can be expressed simply as Eq. (16). In conclusion, FAD installation contributed 9% to the development of the cavitation effect in diesel injection nozzles.

$$y=1.29x^{-1.07} \quad (14)$$

$$y=1.41x^{-1.07} \quad (15)$$

$$y_{FAD}=1.09y \quad (16)$$

4. Evaluation of FAD Effect by Field Experiments

To confirm the combustion improvement by installation of the FAD, an old diesel vehicle (Bongo 3, KIA Motors, Korea) was examined focusing on particulate and nitrogen oxides [39]. Exhausted particles were much more during driving than idling regardless of nozzle configuration, and the reduction effect was maximum 42 w/w%. The release of nitrogen oxides was decreased by 10 to 30 ppm depending on the driving level. A field locomotive train test also was performed in Mongolia, and it resulted in an obvious reduction of fuel consumption [6].

CONCLUSIONS

The present numerical simulation enables one to describe the mechanism inside the fuel injection nozzle responsible for forming cavitation. An auxiliary device, FAD, decreased the potential energy by increasing the eddy viscosity, but reduced the inlet pressure by half compared to the case without FAD. Nevertheless, cavitation was sufficiently formed in the nozzle. In addition, the flow velocity in the nozzle increased by 8.7-times, which may greatly contribute to fuel atomization. Based on the cavitation number ($L=1.41K_2^{-1.07}$), the cavitation was 1.09-times longer with FAD than without. It was proved by field tests using a diesel locomotive and a commercial truck as seen in references [6,34]. In conclusion, the cavitation phenomenon could be theoretically proved by a numerical simulation using a commercial CFD code, and thereby present a clue which can improve combustion efficiency of diesel engines.

ACKNOWLEDGEMENT

This work (No. 20160951) was supported by Business for Cooperative R&D program between Industry, Academy, Research Institute funded by the Korea Small and Medium Business Administration in 2016. Hyun Chang Lee deeply appreciates the support of a 2017 Research Grant from Kangwon National University (No. 201510059).

NOMENCLATURE

B_0 : empirical constant: 0.61
B_2 : empirical constant: 1
Cs : smagorinsky constant
D_n : nozzle diameter [mm]
k : carman constant
L_s : mixing ratio of fine grid
P_{in} : inlet pressure [atm]
P_b : cylinder pressure [atm]
P_c : pressure at a point reduced by axial flow [atm]
p_v : saturated vapor pressure [atm]
p : static pressure [atm]
R_e : generation rate of bubbles
R_c : decay rate of bubbles
Re_1 : Reynolds number
R_B : bubble diameter
T : Taylor number
We_1 : Weber number of liquid
We_2 : Weber number of gas
V_n : liquid average velocity
V : volume of cell grids
V_c : velocity of the point increased by the axial flow
Z : ohnesorge number

Greeks Letters

α : vapor volume fraction
ρ_v : vapor density [kg/m^3]
ρ_l : liquid density [kg/m^3]
Ω : largest growth disturbance
Λ : wave length
μ_l : liquid viscosity [kg/m·s]
κ : cavitation number
σ_l : liquid surface tension

REFERENCES

1. H. K. Suh and C. S. Lee, *Renew. Sust. Energy Rev.*, **58**, 1601 (2016).
2. H. J. Kim, *MA dissertation*, Kyung Hee University, Korea (1997).
3. IARC, Diesel Engine Exhaust Carcinogenic, *International Agency*

of Research on Cancer (2012).
4. S. I. Choi, J. P. Feng, H. S. Seo, S. B. Kim and Y. M. Jo, *J. Korean Soc. Atmos. Environ.*, **33**(4), 306 (2017).
5. Y. S. Lee, *MA dissertation*, Kyung Hee University, Korea (2006).
6. D. S. Park, T. J. Lee, Y. I. Lee, W. S. Jeong, S. B. Kwon, D. S. Kim and K. Y. Lee, *Sci. Total Environ.*, **575**, 97 (2017).
7. S. Ghods, Arizona State University, ProQuest Dissertations Publishing, 3567676 (2013).
8. Z. He, X. Tao, W. Zhong, X. Leng, Q. Wang and P. Zhao, *Int. Communications in Heat and Mass Transfer*, **65**, 117 (2015).
9. B. Yin, S. Yu, H. Jia and J. Yu, *Int. J. Heat Fluid Flow*, **59**, 1 (2016).
10. R. Payri, F. J. Salvador, J. Gimeno and O. Venegas, *Exp. Therm. Fluid Sci.*, **44**, 235 (2013).
11. C. P. Egerer, H. Stefan, J. S. Steffen and A. A. Nikolaus, *Phys. Fluids*, **26**, 085102 (2014).
12. A. Sou, B. Biçer and A. Tomiyama, *Comput. Fluids*, **103**, 42 (2014).
13. S. Yu, B. Yin, H. Jia, S. Wen, X. Li and J. Yu, *Fuel*, **208**, 20 (2017).
14. S. V. Apte, M. Gorokhovski and P. Moin, *Int. J. Multiphase Flow*, **29**, 1503 (2003).
15. W. Yuan, J. Sauer and G. H. Schnerr, *Méc. Ind.*, **2**(5), 383 (2001).
16. Z. He, C. Yuhang, L. Xianyin, W. Qian and G. Genmiao, *Int. Communications in Heat and Mass Transfer*, **76**, 108 (2016).
17. S. K. Park, S. C. Woo, H. G. Kim and K. Y. Lee, *Appl. Energy*, **176**, 209 (2016).
18. F. J. Salvadora, J. V. Romero, M. D. Roselló and D. Jaramillo, *J. Comput. Appl. Mathematics*, **291**, 94 (2016).
19. B. Mohan, W. Yang and S. K. Chou, *Energy Convers. Manage.*, **77**, 269 (2014).
20. M. Ghiji, L. Goldsworthy, P. A. Brandner, V. Garaniya and P. Hield, *Fuel*, **175**, 274 (2016).
21. A. Sou, S. Hosokawa and A. Tomiyama, *Int. J. Heat and Mass Transfer*, **50**, 3575 (2007).
22. R. Pyszczek, Ł. J. Kapusta and A. Teodorczyk, *J. Power Technol.*, **97**(1), 52 (2017).
23. Z. He, Z. Shao, Q. Wang, W. Zhong and X. Tao, *Exp. Therm. Fluid Sci.*, **60**, 252 (2015).
24. A. H. Lefebvre, *Taylor & Francis*, New York (1989).
25. C. Baumgarten, J. Stegemann and G. P. Marker, *Proc. of 18th ILASS Europe Conference*, Zaragoza, Spain, 15 (2002).
26. F. Payri, R. Payri, F. J. Salvador and J. Martínez-López, *Comput. Fluids*, **58**, 88 (2012).
27. W. Bergwerk, *Proc. Institute of Mechanical Engineers*, **173**(25), 655 (1959).
28. C. Soteriou, R. Andrews and M. Smith, *SAE Paper*, Paper No. 950080 (1995).
29. W. H. Nurick, *Trans. ASME*, **98**(4), 681 (1976).
30. F. Payri, V. Bermúdez, R. Payri and F. J. Salvador, *Fuel*, **83**, 419 (2004).
31. H. Hiroyasu, M. Arai and M. Shimizu, *Proceedings of International Conference on Liquid Atomization and Spray Systems*, **91**(ICLASS 91), 275 (1991).
32. T. Qiu, X. Song, Y. Lei, X. Liu, X. An and M. Lai, *Appl. Therm. Eng.*, **109**, 364 (2016).
33. A. Zhandi, S. Sohrabi and M. Shams, *Int. J. Automotive Eng.*, **5**, 940 (2015).
34. S. Som, S. K. Aggarwal, E. M. El-Hannouny and D. E. Longman, *J. Eng. Gas Turbines Power*, **132**(4), 042802 (2010).
35. S. Molina, F. J. Salvador, M. Carreres and D. Jaramillo, *Energy Convers. Manage.*, **79**, 114 (2014).
36. Z. Y. Sun, G. X. Li, C. Chen, Y. S. Yu and G. X. Gao, *Energy Convers. Manage.*, **89**, 843 (2015).
37. F. Wang, Z. He, J. Liu and Q. Wang, *Int. J. Automotive Technol.*, **16**(4), 539 (2015).
38. M. Gavaises, A. Andriotis, D. Papoulias and A. Theodorakakos, *Phys. Fluids*, **21**, 052107 (2017).
39. J. P. Feng, S. I. Choi, H. S. Seo and Y. M. Jo, *Korean J. Chem. Eng.* (2018), DOI:10.1007/s11814-018-0106-9.